(Preprint) AAS 24-021

MODULAR ROTATIONAL STABILITY ANALYSIS OF SPACECRAFT WITH ROTATING FLEXIBLE SOLAR ARRAYS

João Vaz Carneiro[*], Cody Allard[†] and Hanspeter Schaub[‡]

Performing frequency-domain analysis is an important step in the spacecraft design process because it quantifies the impact of flexible structures on the spacecraft's performance and guarantees stability and robustness to unmodeled effects. This is particularly important given the proliferation of big, flexible solar arrays, which are needed for deep-space missions, but that have considerable impacts on the spacecraft's pointing performance. This paper presents an approach to analyzing these effects. It utilizes a novel set of general equations of motion that describe a spacecraft with rotational appendages (also called effectors). These can be used to modularly simulate a system with any number of effectors with different locations, mass properties, and flexing modes without having to rederive the equations each time the spacecraft configuration changes. Therefore, this approach is applicable not to any particular point solution, but rather to a vast number of different possible configurations. The equations of motion of a spacecraft with flexible solar arrays are presented, linearized, discretized, and written into state space form. Then, classical control theory is applied to analyze the frequency response of the system, which includes the study of the Body plots of the open and closed-loop transfer functions, as well as the quantification of the system's gain and phase margins. The mathematical approach to this process is rigorously shown, and a numerical example is provided to illustrate how the approach can be used in a realistic setting.

INTRODUCTION

Flexible structures have always been a part of spacecraft design. From the beginning of the space race, when Sputnik 1 had four large antenna booms to communicate with ground stations, to Lucy's enormous solar arrays, flexible structures have played a key role in many missions. It is essential to include and understand the impact of these flexible structures on the spacecraft's dynamics to predict the craft's behavior and guarantee that the mission requirements are met. However, modeling and analyzing flexible structures is often difficult because closed-form solutions are hard to find, unlike the results for rigid bodies. This results in one of two approaches: simplification of the model, often through limiting assumptions and linearization techniques, or computational analysis, using high-end finite-element computational models that numerically solve the flexible behavior.

Given these challenges, from a guidance, navigation, and control perspective, many spacecraft components are treated as rigid for simulation and analysis. This is usually a fair assumption since

[*]Graduate Research Assistant, Ann and H.J. Smead Department of Aerospace Engineering Sciences, University of Colorado, Boulder, 431 UCB, Colorado Center for Astrodynamics Research, Boulder, CO, 80309.

[†]Guidance, Navigation and Control Engineer, Laboratory for Atmospheric and Space Physics, University of Colorado Boulder, Boulder, CO, 80303 USA

[‡]Professor and Department Chair, Schaden Leadership Chair, Ann and H.J. Smead Department of Aerospace Engineering Sciences, University of Colorado, Boulder, 431 UCB, Colorado Center for Astrodynamics Research, Boulder, CO, 80309. AAS Fellow, AIAA Fellow.

the rigid body modes are far more consequential than the first few flexing modes, and it greatly simplifies the governing equations of motion. However, flexible structure analysis is still essential for many missions where flexible structures cannot be modeled as rigid bodies due to their impact on the spacecraft's performance. In particular, the effects of control-structure interactions[1] must be accounted for. These relate to the coupling between the control effort applied to the spacecraft and its impact on its flexible structures. The control actuators, being discrete devices, excite the system at some discretization frequency. Suppose the control frequency is close to the frequency of one of the flexible structure's natural modes. In that case, the control effort can excite those frequencies, resonating the natural mode and inducing an unstable vibration that can have devastating consequences, such as breaking joints or tearing the structure apart. These interactions depend on the physical properties of the spacecraft, which define the natural frequency of the flexible modes, as well as the controller gains and the sampling frequency.

The field of stability analysis is rich with different techniques used to tackle distinct problems. For linear systems, classical theories[2,3] include Root Locus for closed-loop pole placement and Bode and Nyquist plots for steady-state frequency-response analysis. For nonlinear systems, Lyapunov stability functions[4,5] can be used, while other techniques such as H_∞[2,4] can be used to set up controllers with guaranteed stability metrics. This paper focuses on classical control techniques by linearizing the nonlinear equations of motion.

As for modeling flexible modes, many approaches exist, ranging from simple and robust, albeit not as accurate, to complex and realistic, but lacking closed-form solutions and computationally expensive. These include modeling flexing bodies using the Euler-Bernoulli beam model,[5,6] which has a free closed-form solution, the assumed modes technique,[5] which uses global functions to approximate the problem for geometries that do not have direct closed-form solutions, and the finite element model,[6] which discretizes flexible body into many sections and computationally computes its behavior by taking into account the boundary conditions for each section. This paper models the panel's flexing by approximating it as a rigid body rotating about a very stiff hinge. The hinge's parameters, namely its spring and damper coefficients, depend on the modeled body's natural frequency and damping ratio.

Ref. 7 introduces a novel way of finding the equations of motion of spacecraft composed of rotating appendages attached to a rigid hub. Instead of making assumptions specific to one type of effector, like a reaction wheel or a hinged solar panel, and then deriving the equations of motion (which would be specific to the initial assumptions), the equations are derived in a general way such that they are applicable to rotating appendages with different mass and inertia properties. Ref. 8 expands on this idea by simulating rotating appendages with any number of degrees of freedom, including effectors that have multi-hinged joints between subsections. Moreover, the equations are modular, thanks to the Backsubstitution Method,[9,10] which means that any number of appendages, all with potentially different mass properties and attachment locations, can be simulated at once with this approach. This paper takes this general result and linearizes its equations, retaining the benefits of simulating a large class of spacecraft configurations without having to rederive and linearize the equations each time. These benefits are particularly important in the early phases of mission design, where different configurations can be compared and tested given their performance characteristics.

This work also builds on top of Ref. 11, which defines the formulation of how stability analysis is done by linearizing the governing equations of motion, writing the state-space model, and doing frequency analysis on the resulting system by analyzing Bode plots. This paper expands on that work in a few ways. First, the flexible structures, which consist of solar panels, can rotate about

a hinge, unlike the fixed configuration in previous work. This is in line with new mission designs that allow the solar arrays to autonomously track the sun. However, this complicates the problem since the flexing behavior is not constant as seen from the hub, but changes as the solar arrays rotate about their spin axis. Second, previous work only focuses on a singular flexing mode under the assumption that it has, by far, the most dominant effect on the spacecraft. This paper assumes that the flexible structure has critical flexing modes about any axis (yaw, pitch, and roll), increasing the problem's complexity.

The result of this work is a methodology for finding, linearizing, and discretizing the general equations of motion related to flexible panel dynamics, as well as the approach to interpreting the results from the Bode plots, including stability margins and mode interaction. Ultimately, this approach informs control gain selection for a particular spacecraft configuration and establishes whether performance and stability requirements are met.

This paper is organized as follows. First, the problem statement is presented. Then, the nonlinear equations of motion are derived and linearized by dropping higher-order terms. The linear set of equations of motion is then written into state space form and transformed from the continuous to the discrete domain using a zero-order hold discretization technique.[12] Afterward, the Laplace transform is applied to the discrete state space, which results in open and closed-loop transfer functions. The following section introduces the frequency domain analysis techniques. Finally, a comprehensive numerical simulation is presented, which shows how the analysis is performed with a realistic example.

PROBLEM STATEMENT

The problem statement is illustrated in Figure 1. The inertial frame $\mathcal{N}$ is located at point N. The

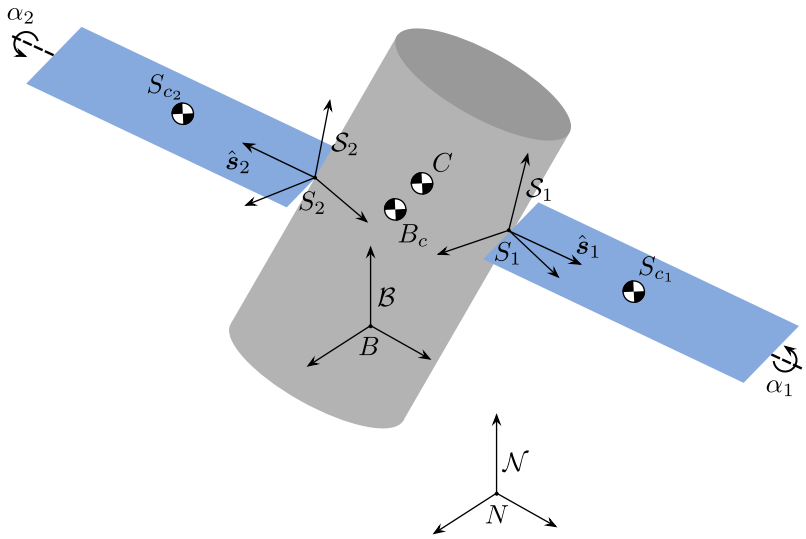

Figure 1: Problem statement.

spacecraft is composed of a rigid hub in gray, with its center of mass at point B_c and a body frame $\mathcal{B}$ at point B. There are two flexible arrays attached to the hub in blue. Each panel has a center of mass S_c and a frame $\mathcal{S}$ located at point S. The solar panels rotate about their spin axis $\hat{\boldsymbol{s}}$ through angle α, and the spin axis goes through point S. The center of mass of the spacecraft is located at

point C.

The solar arrays can flex about any of their principal axes, resulting in three modes: torsional, bending, and pinwheel. Each mode is parameterized by a small angle θ, which is not shown in the diagram. Therefore, the arrays rigidly rotate about their spin axis $\hat{\boldsymbol{s}}$ through angle α and then flex about the rotated frame through angles θ for each mode.

Note that the diagram shown in Figure 1 is simply a general model used to develop the equations of motion. For the numerical example, some assumptions are made about this model. For example, the B and C points are assumed to be aligned, which makes the $\mathcal{B}$ frame located at the spacecraft's center of mass. Another example is that the solar arrays are placed symmetrically about the hub, whereas the problem statement diagram shows that they have an offset. The same can be said for the attitude of the panel's frames.

EQUATIONS OF MOTION

In this section, the equations of motion used for analysis are derived. Since the analysis focuses on the impact and stability of external torques on the system, only the rotational equations are considered. The kinematic and dynamic nonlinear differential equations are shown, which are linearized afterward under the assumption of small angles for the flexing solar arrays.

Kinematic Differential Equations

The chosen attitude parameterization is the Modified Rodrigues Parameters (MRPs) denoted as $\boldsymbol{\sigma}_{\mathcal{B}/\mathcal{N}}$, where $\mathcal{B}$ and $\mathcal{N}$ denote the body and inertial frames, respectively. The kinematic differential equation[5] is

$$\dot{\boldsymbol{\sigma}}_{\mathcal{B}/\mathcal{N}} = \frac{1}{4}[B(\boldsymbol{\sigma}_{\mathcal{B}/\mathcal{N}})]^{\mathcal{B}}\boldsymbol{\omega}_{\mathcal{B}/\mathcal{N}} \tag{1}$$

The other differential equation relates to the hinged bodies and is given by

$$\dot{\theta}_{k,i} = \frac{\mathrm{d}}{\mathrm{d}t}(\theta_{k,i}) \tag{2}$$

where $\theta_{k,i}$ is the i-th flexing angle of the k-th panel.

Dynamic Differential Equations

The development of the equations of motion is shown in Ref. 8, which also details the general problem setup and the assumptions made. The rotational equation of motion for a spacecraft composed of N_s chains of N_k rigid bodies rotating about one-axis hinges and attached to a rigid hub

is

$$
\begin{aligned}
&m_{\mathrm{sc}}[\tilde{\boldsymbol{c}}]\ddot{\boldsymbol{r}}_{B/N} + [I_{\mathrm{sc},B}]\dot{\boldsymbol{\omega}}_{\mathcal{B}/\mathcal{N}} \\
&+\sum_{k=1}^{N_s}\sum_{i=1}^{N_k}\left(\sum_{j=i}^{N_k}\left([I_{\mathrm{S}_{k,j},S_{c_{k,j}}}] - m_{\mathrm{S}_{k,j}}[\tilde{\boldsymbol{r}}_{S_{c_{k,j}}/B}][\tilde{\boldsymbol{r}}_{S_{c_{k,j}}/S_{k,i}}]\right)\right)\hat{\boldsymbol{s}}_{k,i}\ddot{\theta}_{k,i} = \\
&=\boldsymbol{L}_B - [\tilde{\boldsymbol{\omega}}_{\mathcal{B}/\mathcal{N}}][I_{\mathrm{sc},B}]\boldsymbol{\omega}_{\mathcal{B}/\mathcal{N}} - [I'_{\mathrm{sc},B}]\boldsymbol{\omega}_{\mathcal{B}/\mathcal{N}} \\
&-\sum_{k=1}^{N_s}\sum_{i=1}^{N_k}\left([\tilde{\boldsymbol{\omega}}_{\mathcal{S}_{k,i}/\mathcal{N}}][I_{\mathrm{S}_{k,i},S_{c_{k,i}}}]\boldsymbol{\omega}_{\mathcal{S}_{k,i}/\mathcal{B}} - [I_{\mathrm{S}_{k,i},S_{c_{k,i}}}]\sum_{j=1}^{i-1}[\tilde{\boldsymbol{\omega}}_{\mathcal{S}_{k,i}/\mathcal{S}_{k,j}}]\boldsymbol{\omega}_{\mathcal{S}_{k,j}/\mathcal{S}_{k,j-1}}\right) \\
&-\sum_{k=1}^{N_s}\sum_{i=1}^{N_k} m_{\mathrm{S}_{k,i}}[\tilde{\boldsymbol{r}}_{S_{c_{k,i}}/B}]\Bigg([\tilde{\boldsymbol{\omega}}_{\mathcal{B}/\mathcal{N}}][\tilde{\boldsymbol{r}}_{S_{c_{k,i}}/B}]\boldsymbol{r}'_{S_{c_{k,i}}/B} + \sum_{j=1}^{i}[\tilde{\boldsymbol{\omega}}_{\mathcal{S}_{k,j}/\mathcal{S}_{k,j-1}}]\boldsymbol{r}'_{S_{c_{k,i}}/S_{k,j}} \\
&-\sum_{j=1}^{i-1}[\tilde{\boldsymbol{r}}_{S_{c_{k,i}}/S_{k,j+1}}][\tilde{\boldsymbol{\omega}}_{\mathcal{S}_{k,j}/\mathcal{B}}]\boldsymbol{\omega}_{\mathcal{S}_{k,j+1}/\mathcal{S}_{k,j}}\Bigg)
\end{aligned}
\tag{3}
$$

The spinning body equation of motion for the n-th degree of freedom of the k-th chain is

$$
\begin{aligned}
&\hat{\boldsymbol{s}}_{k,n}^T\sum_{i=1}^{n}\left(\sum_{j=n}^{N_k}\left([I_{\mathrm{S}_{k,j},S_{c_{k,j}}}] - m_{\mathrm{S}_{k,j}}[\tilde{\boldsymbol{r}}_{S_{c_{k,j}}/S_{k,n}}][\tilde{\boldsymbol{r}}_{S_{c_{k,j}}/S_{k,i}}]\right)\right)\hat{\boldsymbol{s}}_{k,i}\ddot{\theta}_{k,i} \\
&+\hat{\boldsymbol{s}}_{k,n}^T\sum_{i=n+1}^{N_k}\left(\sum_{j=i}^{N_k}\left([I_{\mathrm{S}_{k,j},S_{c_{k,j}}}] - m_{\mathrm{S}_{k,j}}[\tilde{\boldsymbol{r}}_{S_{c_{k,j}}/S_{k,n}}][\tilde{\boldsymbol{r}}_{S_{c_{k,j}}/S_{k,i}}]\right)\right)\hat{\boldsymbol{s}}_{k,i}\ddot{\theta}_{k,i} = u_{k,n} \\
&-\hat{\boldsymbol{s}}_{k,n}^T\sum_{i=n}^{N_k} m_{\mathrm{S}_{k,i}}[\tilde{\boldsymbol{r}}_{S_{c_{k,i}}/S_{k,n}}]\ddot{\boldsymbol{r}}_{B/N} \\
&-\hat{\boldsymbol{s}}_{k,n}^T\sum_{i=n}^{N_k}\left([I_{\mathrm{S}_{k,i},S_{c_{k,i}}}] - m_{\mathrm{S}_{k,i}}[\tilde{\boldsymbol{r}}_{S_{c_{k,i}}/S_{k,n}}][\tilde{\boldsymbol{r}}_{S_{c_{k,i}}/B}]\right)\dot{\boldsymbol{\omega}}_{\mathcal{B}/\mathcal{N}} \\
&-\hat{\boldsymbol{s}}_{k,n}^T\sum_{i=n}^{N_k}\Big([\tilde{\boldsymbol{\omega}}_{\mathcal{S}_{k,i}/\mathcal{N}}][I_{\mathrm{S}_{k,i},S_{c_{k,i}}}]\boldsymbol{\omega}_{\mathcal{S}_{k,i}/\mathcal{N}} - [I_{\mathrm{S}_{k,i},S_{c_{k,i}}}][\tilde{\boldsymbol{\omega}}_{\mathcal{S}_{k,i}/\mathcal{B}}]\boldsymbol{\omega}_{\mathcal{B}/\mathcal{N}} \\
&\qquad - [I_{\mathrm{S}_{k,i},S_{c_{k,i}}}]\sum_{j=1}^{i-1}[\tilde{\boldsymbol{\omega}}_{\mathcal{S}_{k,i}/\mathcal{S}_{k,j}}]\boldsymbol{\omega}_{\mathcal{S}_{k,j}/\mathcal{S}_{k,j-1}}\Big) \\
&-\hat{\boldsymbol{s}}_{k,n}^T\sum_{i=n}^{N_k} m_{\mathrm{S}_{k,i}}[\tilde{\boldsymbol{r}}_{S_{c_{k,i}}/S_{k,n}}]\Big([\tilde{\boldsymbol{\omega}}_{\mathcal{B}/\mathcal{N}}][\tilde{\boldsymbol{\omega}}_{\mathcal{B}/\mathcal{N}}]\boldsymbol{r}_{S_{c_{k,i}}/B} + 2[\tilde{\boldsymbol{\omega}}_{\mathcal{B}/\mathcal{N}}]\boldsymbol{r}'_{S_{c_{k,i}}/B} \\
&\quad + \sum_{j=1}^{i}[\tilde{\boldsymbol{\omega}}_{\mathcal{S}_{k,j}/\mathcal{S}_{k,j-1}}]\boldsymbol{r}'_{S_{c_{k,i}}/S_{k,j}} - \sum_{j=1}^{i-1}[\tilde{\boldsymbol{r}}_{S_{c_{k,i}}/S_{k,j+1}}][\tilde{\boldsymbol{\omega}}_{\mathcal{S}_{k,j}/\mathcal{B}}]\boldsymbol{\omega}_{\mathcal{S}_{j+1}/\mathcal{S}_{k,j}}\Big)
\end{aligned}
\tag{4}
$$

Linearization

Linearizing simplifies the equations by dropping higher-order terms, assuming they are smaller than lower-order terms. The linearization process also produces linear equations, which can be put

into state space form to apply control theories. For the kinematic differential equations, the MRPs equation simplifies to

$$\dot{\boldsymbol{\sigma}}_{\mathcal{B}/\mathcal{N}} = \frac{1}{4}{}^{\mathcal{B}}\boldsymbol{\omega}_{\mathcal{B}/\mathcal{N}} \tag{5}$$

This is because for small values of $\boldsymbol{\sigma}_{\mathcal{B}/\mathcal{N}}$, the $[B(\boldsymbol{\sigma}_{\mathcal{B}/\mathcal{N}})]$ matrix simplifies to the identity matrix. See Ref. 5 for more details. The other kinematics differential equation is unchanged, which means

$$\dot{\theta}_{k,i} = \frac{\mathrm{d}}{\mathrm{d}t}(\theta_{k,i}) \tag{6}$$

All implicit second-order terms are ignored to linearize the dynamic equations of motion. These correspond to terms that do not explicitly depend on the second-order state derivatives, namely $\dot{\boldsymbol{\omega}}_{\mathcal{B}/\mathcal{N}}$ and $\ddot{\theta}_{k,i}$. Moreover, it is assumed that the origin of the $\mathcal{B}$ frame B coincides with the center of mass of the spacecraft C ($\boldsymbol{c} = \boldsymbol{r}_{B/C} = \boldsymbol{0}$) and that there is no translational motion $\ddot{\boldsymbol{r}}_{B/N} = \boldsymbol{0}$.

$$\begin{aligned}
&\cancel{m_{\mathrm{sc}}[\tilde{\boldsymbol{c}}]\ddot{\boldsymbol{r}}_{B/N}} + [I_{\mathrm{sc},B}]\dot{\boldsymbol{\omega}}_{\mathcal{B}/\mathcal{N}} \\
&+\sum_{k=1}^{N_s}\sum_{i=1}^{N_k}\left(\sum_{j=i}^{N_k}\left([I_{\mathrm{S}_{k,j},S_{c_{k,j}}}] - m_{\mathrm{S}_{k,j}}[\tilde{\boldsymbol{r}}_{S_{c_{k,j}}/B}][\tilde{\boldsymbol{r}}_{S_{c_{k,j}}/S_{k,i}}]\right)\right)\hat{\boldsymbol{s}}_{k,i}\ddot{\theta}_{k,i} = \\
&=\boldsymbol{L}_B - \cancel{[\tilde{\boldsymbol{\omega}}_{\mathcal{B}/\mathcal{N}}][I_{\mathrm{sc},B}]\boldsymbol{\omega}_{\mathcal{B}/\mathcal{N}}} - \cancel{[I'_{\mathrm{sc},B}]\boldsymbol{\omega}_{\mathcal{B}/\mathcal{N}}} \\
&-\sum_{k=1}^{N_s}\sum_{i=1}^{N_k}\left(\cancel{[\tilde{\boldsymbol{\omega}}_{\mathcal{S}_{k,i}/\mathcal{N}}][I_{\mathrm{S}_{k,i},S_{c_{k,i}}}]\boldsymbol{\omega}_{\mathcal{S}_{k,i}/\mathcal{B}}} - [I_{\mathrm{S}_{k,i},S_{c_{k,i}}}]\sum_{j=1}^{i-1}\cancel{[\tilde{\boldsymbol{\omega}}_{\mathcal{S}_{k,i}/\mathcal{S}_{k,j}}]\boldsymbol{\omega}_{\mathcal{S}_{k,j}/\mathcal{S}_{k,j-1}}}\right) \\
&-\sum_{k=1}^{N_s}\sum_{i=1}^{N_k} m_{\mathrm{S}_{k,i}}[\tilde{\boldsymbol{r}}_{S_{c_{k,i}}/B}]\left(\cancel{[\tilde{\boldsymbol{\omega}}_{\mathcal{B}/\mathcal{N}}][\tilde{\boldsymbol{r}}_{S_{c_{k,i}}/B}]\boldsymbol{r}'_{S_{c_{k,i}}/B}} + \sum_{j=1}^{i}\cancel{[\tilde{\boldsymbol{\omega}}_{\mathcal{S}_{k,j}/\mathcal{S}_{k,j-1}}]\boldsymbol{r}'_{S_{c_{k,i}}/S_{k,j}}}\right. \\
&\left.-\sum_{j=1}^{i-1}\cancel{[\tilde{\boldsymbol{r}}_{S_{c_{k,i}}/S_{k,j+1}}][\tilde{\boldsymbol{\omega}}_{\mathcal{S}_{k,j}/\mathcal{B}}]\boldsymbol{\omega}_{\mathcal{S}_{k,j+1}/\mathcal{S}_{k,j}}}\right)
\end{aligned} \tag{7}$$

which results in

$$[I_{\mathrm{sc},B}]\dot{\boldsymbol{\omega}}_{\mathcal{B}/\mathcal{N}} + \sum_{k=1}^{N_s}\sum_{i=1}^{N_k}\left(\sum_{j=i}^{N_k}\left([I_{\mathrm{S}_{k,j},S_{c_{k,j}}}] - m_{\mathrm{S}_{k,j}}[\tilde{\boldsymbol{r}}_{S_{c_{k,j}}/B}][\tilde{\boldsymbol{r}}_{S_{c_{k,j}}/S_{k,i}}]\right)\right)\hat{\boldsymbol{s}}_{k,i}\ddot{\theta}_{k,i} = \boldsymbol{L}_B \tag{8}$$

The equation above can be further simplified. First, only three degrees of freedom are of concern (torsional, bending, and pinwheel), which means that $N_k = 3$. Second, each panel is composed of a single body, which means that $[I_{\mathrm{S}_{k,j},S_{c_{k,j}}}]$ and m_{S_j} are zero when $j \neq 3$. Finally, there are two panels attached to the same hub. Applying these simplifications

$$[I_{\mathrm{sc},B}]\dot{\boldsymbol{\omega}}_{\mathcal{B}/\mathcal{N}} + \sum_{k=1}^{N_s}\sum_{i=1}^{3}\left([I_{\mathrm{S}_k,S_{c_k}}] - m_{\mathrm{S}_k}[\tilde{\boldsymbol{r}}_{S_{c_k}/B}][\tilde{\boldsymbol{r}}_{S_{c_k}/S_k}]\right)\hat{\boldsymbol{s}}_{k,i}\ddot{\theta}_{k,i} = \boldsymbol{L}_B \tag{9}$$

Following the same linearization techniques for the spinning body equation

$$
\begin{aligned}
&\hat{\boldsymbol{s}}_{k,n}^T \sum_{i=1}^{n} \left(\sum_{j=n}^{N_k} \left([I_{\mathrm{S}_{k,j},S_{c_{k,j}}}] - m_{\mathrm{S}_{k,j}} [\tilde{\boldsymbol{r}}_{S_{c_{k,j}}/S_{k,n}}][\tilde{\boldsymbol{r}}_{S_{c_{k,j}}/S_{k,i}}] \right) \right) \hat{\boldsymbol{s}}_{k,i} \ddot{\theta}_{k,i} \\
&+ \hat{\boldsymbol{s}}_{k,n}^T \sum_{i=n+1}^{N_k} \left(\sum_{j=i}^{N_k} \left([I_{\mathrm{S}_{k,j},S_{c_{k,j}}}] - m_{\mathrm{S}_{k,j}} [\tilde{\boldsymbol{r}}_{S_{c_{k,j}}/S_{k,n}}][\tilde{\boldsymbol{r}}_{S_{c_{k,j}}/S_{k,i}}] \right) \right) \hat{\boldsymbol{s}}_{k,i} \ddot{\theta}_{k,i} = u_{k,n} \\
&- \hat{\boldsymbol{s}}_{k,n}^T \sum_{i=n}^{N_k} m_{\mathrm{S}_{k,i}} [\tilde{\boldsymbol{r}}_{S_{c_{k,i}}/S_{k,n}}] \ddot{\boldsymbol{r}}_{B/N} \\
&- \hat{\boldsymbol{s}}_{k,n}^T \sum_{i=n}^{N_k} \left([I_{\mathrm{S}_{k,i},S_{c_{k,i}}}] - m_{\mathrm{S}_{k,i}} [\tilde{\boldsymbol{r}}_{S_{c_{k,i}}/S_{k,n}}][\tilde{\boldsymbol{r}}_{S_{c_{k,i}}/B}] \right) \dot{\boldsymbol{\omega}}_{\mathcal{B}/\mathcal{N}} \\
&- \hat{\boldsymbol{s}}_{k,n}^T \sum_{i=n}^{N_k} \Big([\tilde{\boldsymbol{\omega}}_{\mathcal{S}_{k,i}/\mathcal{N}}][I_{\mathrm{S}_{k,i},S_{c_{k,i}}}] \boldsymbol{\omega}_{\mathcal{S}_{k,i}/\mathcal{N}} - [I_{\mathrm{S}_{k,i},S_{c_{k,i}}}][\tilde{\boldsymbol{\omega}}_{\mathcal{S}_{k,i}/\mathcal{B}}] \boldsymbol{\omega}_{\mathcal{B}/\mathcal{N}} \\
&\quad - [I_{\mathrm{S}_{k,i},S_{c_{k,i}}}] \sum_{j=1}^{i-1} [\tilde{\boldsymbol{\omega}}_{\mathcal{S}_{k,i}/\mathcal{S}_{k,j}}] \boldsymbol{\omega}_{\mathcal{S}_{k,j}/\mathcal{S}_{k,j-1}} \Big) \\
&- \hat{\boldsymbol{s}}_{k,n}^T \sum_{i=n}^{N_k} m_{\mathrm{S}_{k,i}} [\tilde{\boldsymbol{r}}_{S_{c_{k,i}}/S_{k,n}}] \Big([\tilde{\boldsymbol{\omega}}_{\mathcal{B}/\mathcal{N}}][\tilde{\boldsymbol{\omega}}_{\mathcal{B}/\mathcal{N}}] \boldsymbol{r}_{S_{c_{k,i}}/B} + 2[\tilde{\boldsymbol{\omega}}_{\mathcal{B}/\mathcal{N}}] \boldsymbol{r}'_{S_{c_{k,i}}/B} \\
&\quad + \sum_{j=1}^{i} [\tilde{\boldsymbol{\omega}}_{\mathcal{S}_{k,j}/\mathcal{S}_{k,j-1}}] \boldsymbol{r}'_{S_{c_{k,i}}/S_{k,j}} - \sum_{j=1}^{i-1} [\tilde{\boldsymbol{r}}_{S_{c_{k,i}}/S_{k,j+1}}][\tilde{\boldsymbol{\omega}}_{\mathcal{S}_{k,j}/\mathcal{B}}] \boldsymbol{\omega}_{\mathcal{S}_{j+1}/\mathcal{S}_{k,j}} \Big)
\end{aligned}
\tag{10}
$$

which results in

$$
\begin{aligned}
&\hat{\boldsymbol{s}}_{k,n}^T \sum_{i=1}^{n} \left(\sum_{j=n}^{N_k} \left([I_{\mathrm{S}_{k,j},S_{c_{k,j}}}] - m_{\mathrm{S}_{k,j}} [\tilde{\boldsymbol{r}}_{S_{c_{k,j}}/S_{k,n}}][\tilde{\boldsymbol{r}}_{S_{c_{k,j}}/S_{k,i}}] \right) \right) \hat{\boldsymbol{s}}_{k,i} \ddot{\theta}_{k,i} \\
&+ \hat{\boldsymbol{s}}_{k,n}^T \sum_{i=n+1}^{N_k} \left(\sum_{j=i}^{N_k} \left([I_{\mathrm{S}_{k,j},S_{c_{k,j}}}] - m_{\mathrm{S}_{k,j}} [\tilde{\boldsymbol{r}}_{S_{c_{k,j}}/S_{k,n}}][\tilde{\boldsymbol{r}}_{S_{c_{k,j}}/S_{k,i}}] \right) \right) \hat{\boldsymbol{s}}_{k,i} \ddot{\theta}_{k,i} = u_{k,n} \\
&- \hat{\boldsymbol{s}}_{k,n}^T \sum_{i=n}^{N_k} \left([I_{\mathrm{S}_{k,i},S_{c_{k,i}}}] - m_{\mathrm{S}_{k,i}} [\tilde{\boldsymbol{r}}_{S_{c_{k,i}}/S_{k,n}}][\tilde{\boldsymbol{r}}_{S_{c_{k,i}}/B}] \right) \dot{\boldsymbol{\omega}}_{\mathcal{B}/\mathcal{N}}
\end{aligned}
\tag{11}
$$

Further simplifying results in

$$
\begin{aligned}
&\hat{\boldsymbol{s}}_{k,n}^T \left([I_{\mathrm{S}_k,S_{c_k}}] - m_{\mathrm{S}_k} [\tilde{\boldsymbol{r}}_{S_{c_k}/S_k}][\tilde{\boldsymbol{r}}_{S_{c_k}/B}] \right) \dot{\boldsymbol{\omega}}_{\mathcal{B}/\mathcal{N}} \\
&+ \hat{\boldsymbol{s}}_{k,n}^T \sum_{i=1}^{3} \left([I_{\mathrm{S}_k,S_{c_k}}] - m_{\mathrm{S}_k} [\tilde{\boldsymbol{r}}_{S_{c_k}/S_k}][\tilde{\boldsymbol{r}}_{S_{c_k}/S_k}] \right) \hat{\boldsymbol{s}}_{k,i} \ddot{\theta}_{k,i} = u_{k,n}
\end{aligned}
\tag{12}
$$

In this analysis, the torque $u_{k,n}$ is used to model the natural frequency and damping ratio through spring and damper coefficients $k_{k,n}$ and $c_{k,n}$, respectively.

$$
u_{k,n} = -k_{k,n} \theta_{k,n} - c_{k,n} \dot{\theta}_{k,n} \tag{13}
$$

State Space Representation

The linearization process yields a set of linear differential equations that can be put into a state space model, representing the equations of motion as a set of first-order equations written in matrix and vector form. These matrix equations define how the derivative of the state vector, which contains all state variables that define the system of interest, changes depending on the current state vector and the control vector as an input. The canonical state space representation using a mass matrix is given by

$$[M]\dot{\boldsymbol{X}} = [A]\boldsymbol{X} + [B]\boldsymbol{u} \tag{14}$$

where $\boldsymbol{X}$ is the state vector, $\boldsymbol{u}$ is the control vector, $[M]$ is the system's mass matrix, $[A]$ is the state matrix and $[B]$ is the control matrix. For this problem, the state vector is

$$\boldsymbol{X} = \begin{bmatrix} \boldsymbol{\sigma}_{\mathcal{B}/\mathcal{N}} \\ \boldsymbol{\omega}_{\mathcal{B}/\mathcal{N}} \\ \theta_{1,1} \\ \dot{\theta}_{1,1} \\ \vdots \\ \theta_{2,3} \\ \dot{\theta}_{2,3} \end{bmatrix} \tag{15}$$

Control techniques require that the state vector derivative be solved explicitly, which means that the system's mass matrix must be inverted as follows

$$\dot{\boldsymbol{X}} = [M]^{-1}[A]\boldsymbol{X} + [M]^{-1}[B]\boldsymbol{u} \tag{16}$$

$$= [\tilde{A}]\boldsymbol{X} + [\tilde{B}]\boldsymbol{u} \tag{17}$$

Here, the $[\tilde{A}] = [M]^{-1}[A]$ and $[\tilde{B}] = [M]^{-1}[B]$ matrices become the new state and control matrices. In this case, the control vector corresponds to an external torque on the entire spacecraft, which only directly affects the derivative of the hub's angular velocity. This is done through the control matrix $[B]$, which directs the control vector to the right set of equations.

Discretization

The state space model described before yields linear differential equations in the continuous time domain. However, the controller onboard a spacecraft's computer runs at a discrete rate $f_s = 1/T_s$, where T_s corresponds to the sampling interval of the controller, which means the equations of motion must be transformed to the discrete time domain. The state space formulation is similar in the continuous and discrete time domains, with a few differences. First, the state derivative is replaced by the state vector at the next time step. Second, the state and control matrices change from the continuous time domain, mainly because they now depend on the sampling interval T_s.

The discrete-time state space formulation at the k-th timestep is

$$\boldsymbol{X}(k+1) = [F]\boldsymbol{X}(k) + [G]\boldsymbol{u}(k) \tag{18}$$

with the new matrices being given by

$$[F] = e^{[\tilde{A}]T_s}, \qquad [G] = \left[\int_0^{T_s} e^{[\tilde{A}](T_s-\tau)\mathrm{d}\tau}\right][\tilde{B}] \tag{19}$$

A useful property to find the $[F]$ and $[G]$ matrices without computing integrals can be found in Ref. 13 and is

$$e^{\begin{bmatrix}[\tilde{A}] & [\tilde{B}] \\ [0] & [0]\end{bmatrix}T_s} = \begin{bmatrix}[F] & [G] \\ [0] & [I]\end{bmatrix} \tag{20}$$

Laplace Transform

The next step is to apply the Laplace Transform,[3] an integral transformation commonly used to solve linear differential equations. The Laplace transform is that it has a real domain and a complex codomain. The benefit of the Laplace Transform is that it reduces the set of differential equations in the t time domain to a set of algebraic equations in the s or z domains, depending on whether the system is continuous or discrete, respectively. This is advantageous because algebraic equations are easier to solve than differential equations, which are notoriously difficult to find solutions for. In this application, the Laplace Transform is used for frequency domain analysis, which focuses on the system's steady-state response to sinusoidal inputs to understand the stability margins and response of the system to different frequencies. The z variable relates to the frequency of the sinusoidal input f through

$$z = e^{j2\pi f T_s} \tag{21}$$

The z-domain Laplace transform of this system is

$$z\boldsymbol{X}(z) = [F]\boldsymbol{X}(z) + [G]\boldsymbol{u}(z) \tag{22}$$

which can be solved for $\boldsymbol{X}(z)$ as

$$\boldsymbol{X}(z) = \left(z[I_{N\times N}] - [F]\right)^{-1}[G]\boldsymbol{u}(z) \tag{23}$$

This result establishes a direct correspondence between the input control vector $\boldsymbol{u}(z)$ and the output state vector $\boldsymbol{X}(z)$.

Often, it is convenient to map a reference state to the control vector, which is done by including a gain matrix $[K]$. This is called an open-loop control strategy because the control input does not depend on the current state, only on the predetermined reference state, and $\boldsymbol{u}$ is defined as

$$\boldsymbol{u} = [K]\boldsymbol{X}_{\text{ref}} \tag{24}$$

where $\boldsymbol{X}_{\text{ref}}$ is the reference state vector. When applied to Equation 23, it becomes

$$\boldsymbol{X}(z) = \left(z[I_{N\times N}] - [F]\right)^{-1}[G][K]\boldsymbol{X}_{\text{ref}}(z) = [H](z)\boldsymbol{X}_{\text{ref}}(z) \tag{25}$$

where we define the open-loop transfer function $[H](z)$ as

$$[H](z) = \left(z[I_{N\times N}] - [F]\right)^{-1}[G][K] \tag{26}$$

In practice, the control input depends on the error or difference between the current state and the reference state: $\boldsymbol{u}(s) = [K]\left(\boldsymbol{X}_{\text{ref}} - \boldsymbol{X}\right)$. This is called closed-loop control since there is negative feedback of the state onto the control input. Applying this control law to Equation 23, it becomes

$$\boldsymbol{X}(z) = \left(z[I_{N\times N}] - [F]\right)^{-1}[G][K]\left(\boldsymbol{X}_{\text{ref}}(z) - \boldsymbol{X}(z)\right) \tag{27}$$

which, if you solve for $\boldsymbol{X}(z)$ yields

$$\boldsymbol{X}(z) = (z[I_{N\times N}] - [F] + [G][K])^{-1}[G][K]\boldsymbol{X}_{\text{ref}}(z) = [\tilde{H}](z)\boldsymbol{X}_{\text{ref}}(z) \tag{28}$$

where the closed-loop transfer function $[\tilde{H}](z)$ is defined as

$$[\tilde{H}](z) = (z[I_{N\times N}] - [F] + [G][K])^{-1}[G][K] \tag{29}$$

A very important result is that it can be shown that the open and closed-loop functions are related through the following equation

$$[\tilde{H}](z) = ([I_{N\times N}] + [H](z))^{-1}[H](z) \tag{30}$$

FREQUENCY DOMAIN ANALYSIS

The frequency domain analysis aims to understand the system's steady-state response to sinusoidal inputs. If the system has an undesirable response to certain frequencies, then the spacecraft could become compromised in the event of external perturbations at those frequencies. Some examples include:

1. The system has an unstable response to a particular frequency. When it is excited at that rate, the magnitude of the response increases over time.
2. The system tracks high-frequency inputs with little to no damping. This can lead to the flexible structures oscillating too fast, which is problematic.

Frequency domain analysis can help understand whether the system suffers from these problems. Two types of analysis are performed, which solve each of the examples above: open-loop and closed-loop analysis. Note that while the analysis uses open or closed-loop transfer functions, the goal is always to characterize the system's closed-loop response.

Open-Loop Analysis

Open-loop analysis describes the system's robustness to becoming unstable. For a given $[K]$ gain matrix, the open-loop analysis can quantify how close the system is to becoming unstable. This is important because the model used for analysis is always different from reality. Therefore, it is necessary to have sufficient margin to be confident that the real system will not become unstable.

To perform this analysis, the starting point is Equation 29, which relates the open-loop transfer function $[H]$ to the closed-loop transfer function $[\tilde{H}]$. Note how the closed-loop transfer function depends on the inverse of $[I_{N\times N}] + [H](z)$. If this matrix is singular, the closed-loop transfer function blows up, and the system becomes unstable.

For simplicity, let us assume that the matrix has size one. The instability would occur when $H(z) = -1$ which, since the domain of $H(z)$ is complex, is equivalent to $|H(z)| = 1$ and $\arg(H(z)) = -180°$. Therefore, the open-loop analysis quantifies how close the open-loop transfer function is to $H(z) = -1$ for a range of frequencies. Two quantities are analyzed: the gain margin and the phase margin. Both quantities quantify how much the system can change before it becomes unstable.

1. The **gain margin** describes how much the magnitude of the system's response can change when $\arg(H(z)) = -180^\circ$ before it reaches a value of 1.

2. The **phase margin** describes how much the phase of the system's response can change when $|H(z)| = 1$ before it reaches a value of -180°.

The gain and phase margins are often extracted from a Bode plot, a graph of the magnitude and phase of the system's response to a frequency input. The gain plot represents the magnitude of the response, usually expressed in dB, whereas the phase plot represents the phase of the response, usually in degrees between -180° and 180°. The frequency input is often expressed in a logarithmic scale.

Closed-Loop Analysis

Closed-loop analysis directly describes the system's response to a sinusoidal control input. It analyzes the Bode plot of the closed-loop transfer function $[\tilde{H}](z)$, which quantifies the steady-state magnitude and phase of the system for a range of frequencies. This analysis does not characterize the stability of the closed-loop system; instead, it quantifies how the system reacts after the transient response has subsided.

NUMERICAL EXAMPLE

This section aims to provide an example scenario that uses the approach described in this paper. The analysis techniques described in the previous section are shown by simulating a realistic setting, including many subtleties that can only be discussed with an example case.

Simulation Setup

The hub is a rigid body with mass and inertia properties described in Table 1. The center of mass of the hub is assumed to coincide with the origin of the body frame $\mathcal{B}$, a common assumption in dynamic systems.

Table 1: Simulation parameters for the rigid hub.

Parameter	Notation	Value	Units
Hub's mass	m_{hub}	1000	kg
Hub's inertia about the hub's center of mass	${}^{\mathcal{B}}[I_{\text{hub},B_c}]$	${}^{\mathcal{B}}\begin{bmatrix} 800 & 0 & 0 \\ 0 & 1000 & 0 \\ 0 & 0 & 900 \end{bmatrix}$	kg$\cdot$ m^2
Hub's center of mass location with respect to B	${}^{\mathcal{B}}\boldsymbol{r}_{B_c/B}$	${}^{\mathcal{B}}[0,0,0]^T$	m

Attached to the hub are two identical flexing solar panels. The panels can rotate about the $\hat{\boldsymbol{s}}$ spin axis to better track the Sun. Each solar panel's mass and inertia properties are described in Table 2. The solar arrays are flexible about all three axes, corresponding to the following modes: bending, torsional, and pinwheel. The bending mode rotates about the panel's X axis, the torsional mode about the Y axis, and the pinwheel about the Z axis. Each mode is described by a Q-factor and a natural frequency ω, which go into the spring and damper coefficients k and c, respectively. The k

Table 2: Simulation parameters for the two-panel simulation.

Parameter	Notation	Value	Units
Panel 1's mass	m_{S_1}	20	kg
Panel 2's mass	m_{S_2}	20	kg
Panel 1's inertia about its center of mass	$^{\mathcal{S}_1}[I_{\mathrm{S}_1,S_{c_1}}]$	$^{\mathcal{S}_1}\begin{bmatrix}150 & 0 & 0\\ 0 & 100 & 0\\ 0 & 0 & 200\end{bmatrix}$	kg$\cdot$ m^2
Panel 2's inertia about its center of mass	$^{\mathcal{S}_2}[I_{\mathrm{S}_2,S_{c_2}}]$	$^{\mathcal{S}_2}\begin{bmatrix}150 & 0 & 0\\ 0 & 100 & 0\\ 0 & 0 & 200\end{bmatrix}$	kg$\cdot$ m^2
Panel 1's center of mass location with respect to S_1	$^{\mathcal{S}_1}\boldsymbol{r}_{S_{c_1}/S_1}$	$^{\mathcal{S}_1}[0, 2.5, 0]^T$	m
Panel 2's center of mass location with respect to S_2	$^{\mathcal{S}_2}\boldsymbol{r}_{S_{c_2}/S_2}$	$^{\mathcal{S}_2}[0, 2.5, 0]^T$	m
Position of the origin of the S_1 frame relative to B	$^{\mathcal{B}}\boldsymbol{r}_{S_1/B}$	$^{\mathcal{B}}[0.75, 0, 0]^T$	m
Position of the origin of the S_2 frame relative to B	$^{\mathcal{B}}\boldsymbol{r}_{S_2/B}$	$^{\mathcal{B}}[-0.75, 0, 0]^T$	m
DCM of the S_1 equilibrium frame with respect to the B frame	$[S_{01}B]$	$\begin{bmatrix}0 & 1 & 0\\ 0 & 0 & -1\\ -1 & 0 & 0\end{bmatrix}$	–
DCM of the S_2 equilibrium frame with respect to the B frame	$[S_{02}B]$	$\begin{bmatrix}0 & -1 & 0\\ 0 & 0 & -1\\ 1 & 0 & 0\end{bmatrix}$	–
Rotation axis for S_1	$^{\mathcal{B}}\hat{s}_1$	$^{\mathcal{B}}[1, 0, 0]^T$	–
Rotation axis for S_2	$^{\mathcal{B}}\hat{s}_2$	$^{\mathcal{B}}[-1, 0, 0]^T$	–

and c parameters create the system's state matrix and impact the system's frequency response. The equations that relate these quantities for the n-th mode of the k-th panel are

$$k_{k,n} = I_{k,n}\omega_n^2 \qquad c_{k,n} = I_{k,n}\frac{\omega_n}{Q} \tag{31}$$

where $I_{k,n} = \hat{\boldsymbol{s}}_{k,n}^T[I_{\mathrm{S}_k,S_k}]\hat{\boldsymbol{s}}_{k,n}$ is the inertia fraction of the n-th mode taken at the hinge point S_k, not the center of mass. The values of Q and ω_n for each mode are summarized in Table 3.

Table 3: Properties of each panel's flexible mode.

		Parameter	
		Q	ω
Mode	Bending	30	0.97 Hz
	Torsional	30	0.85 Hz
	Pinwheel	30	0.72 Hz

The control law depends on what axis is being analyzed. From Equation 26, the gain matrix $[K]$ determines the open-loop transfer function. For this analysis, the gain matrix is chosen such that only the attitude and angular velocity components corresponding to the i-th axis are used, which is equivalent to the following control law

$$u_i = -K_1\Delta\sigma_i(z) - K_2\Delta\omega_i(z) \tag{32}$$

where the other two components are 0. This results in a $[K]$ matrix of mostly zeros except for two values corresponding to the i-th attitude and angular velocity components. The gain values used for this analysis are $K_1 = 175$ and $K_2 = 5000$.

The reference state also needs some consideration. Since the angular velocity ω_i is dependent on the derivative of the attitude σ_i, these two quantities are coupled in the z-domain, and it can be shown that they are related through the following expression

$$\omega_i(z) = 4\frac{\ln z}{T_s}\sigma_i(z) \tag{33}$$

with $T_s = 0.1$s. This is not only because the derivative of $\boldsymbol{X}$ in the t domain $\dot{\boldsymbol{X}}$ becomes $\frac{\ln z}{T_s}\boldsymbol{X}$ in the z domain, but also due to the linearized relationship between the derivative of the MRP attitude and the angular velocity $\boldsymbol{\omega} = 4\dot{\boldsymbol{\sigma}}$. For example, if the first axis is to be analyzed, the reference state becomes

$$\boldsymbol{X}_{\text{ref}} = \begin{bmatrix} \sigma_{\text{ref}}(z) \\ 0 \\ 0 \\ 4\frac{\ln z}{T_s}\sigma_{\text{ref}}(z) \\ 0 \\ 0 \\ \vdots \\ 0 \end{bmatrix} = \begin{bmatrix} 1 \\ 0 \\ 0 \\ 4\frac{\ln z}{T_s} \\ 0 \\ 0 \\ \vdots \\ 0 \end{bmatrix} \sigma_{\text{ref}}(z) \tag{34}$$

Therefore, the coupling between the attitude and angular velocity leads to a one-dimensional control input. Moreover, since the analysis is done per each axis, the desired output is the attitude component of the axis of interest, which is also one-dimensional. As a result, the analysis is single-input and single-output (SISO), which means a single Bode plot can be used to analyze each axis.

Open-Loop Analysis

The open-loop analysis focuses on studying the Bode plots for each body axis, shown in Figure 2. Three Bode plots are shown, one for each axis. The Bode plot consists of two graphs: the top one represents the magnitude of the transfer function with respect to the input frequency, and the bottom one represents the phase of the transfer function in terms of the input frequency.

Studying the plots, there are some noticeable similarities between all three.

1. For small frequencies, the slope of the gain is -40dB/decade, which is consistent with a double pure integrator. At low frequencies, the output is simply the second integral of the input since the input affects the derivative of the angular velocity, and the output is the attitude. The response is also completely out of phase since it is at $-180°$.

2. There are artifacts in both magnitude and phase plots for higher frequencies. This is due to the discretization of the state space at $f_s = 10$Hz, with a corresponding Nyquist frequency of 5Hz. Therefore, the response is only valid for input frequencies below 5Hz, and the artifacts seen for larger frequencies do not represent the system's behavior. Interestingly, at the end, the graphs look symmetrical about the sampling frequency of 10Hz, consistent with the expected folding and aliasing of the signal.

The impact of the flexing modes on the Bode plots is shown in Figure 3, which is a zoomed-in view of the Bode plots in Figure 2.

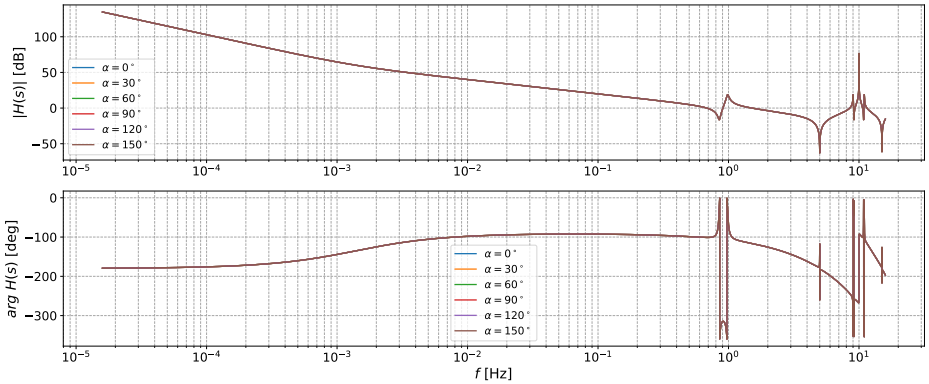

(a) Bode plot for the X axis.

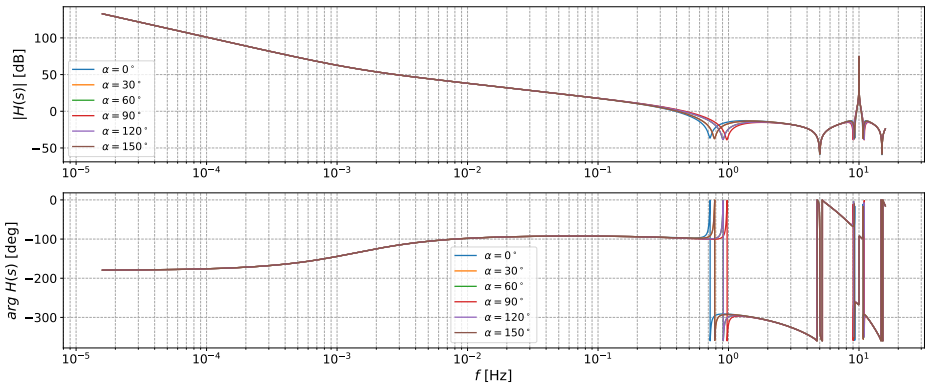

(b) Bode plot for the Y axis.

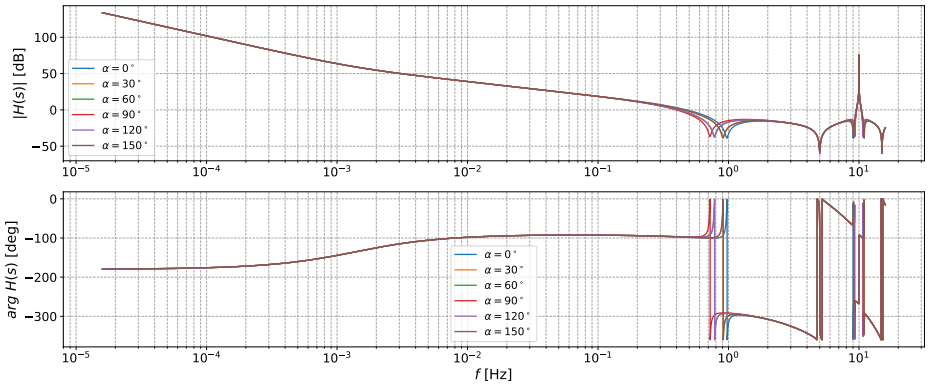

(c) Bode plot for the Z axis.

Figure 2: Bode plot of the open-loop transfer function for each axis.

1. The response on the X axis is shown in Figure 3a. It shows that the response is the same for all rotation angles of the solar arrays. This is because the rotating solar array axis is along the body's X axis, which means that changing the angle does not impact the system's response. Moreover, the gain plot dips at $f = 0.85$Hz, corresponding to the torsional mode's natural frequency, consistent with spinning about the torsional axis.

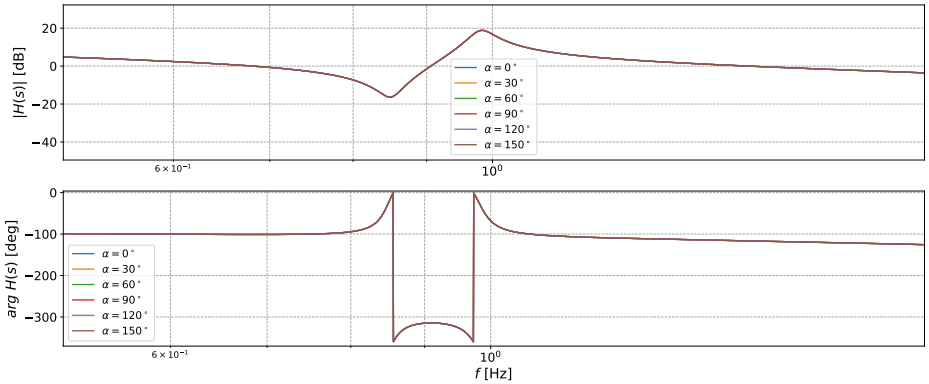

(a) Bode plot for the X axis.

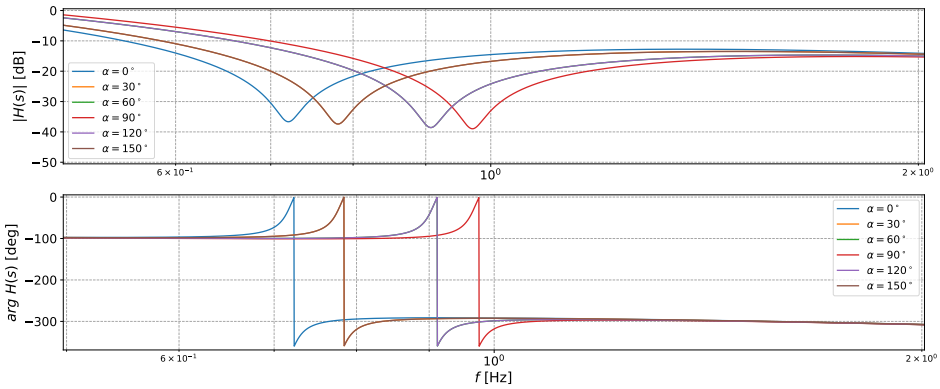

(b) Bode plot for the Y axis.

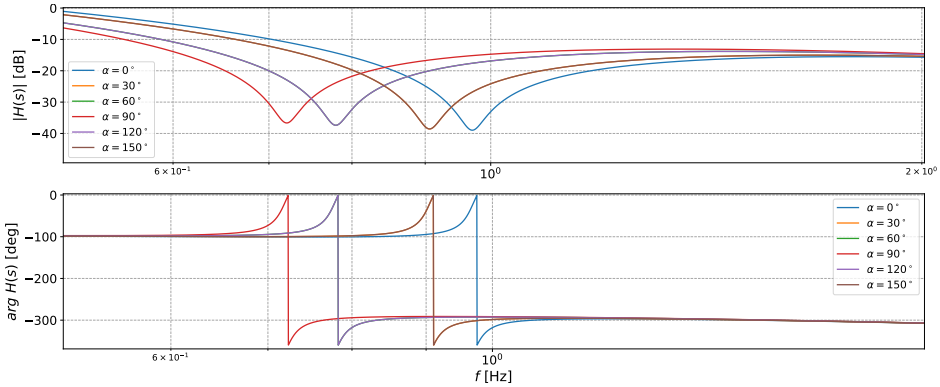

(c) Bode plot for the Z axis.

Figure 3: Bode plot of the open-loop transfer function for each axis.

2. The response on the Y axis is shown in Figure 3b. Here, the solar array rotation angles have an impact on the frequency response of the system. For $\alpha = 0°$, the mode is excited at $f = 0.72$Hz, consistent with the pinwheel mode. This happens when the panel's normal faces the Y axis, and the solar arrays flex sideways. For $\alpha = 90°$, the mode is excited at $f = 0.97$Hz, corresponding to the bending mode. This occurs when the panel's normal faces

the Z axis, and the solar arrays flex up and down. The frequency response is a mix of bending and pinwheel responses for intermediate angles, which is why the characteristic frequency is between the two values.

3. The response on the Z axis is shown in Figure 3c. The system's behavior is very similar to the one seen for the Y axis but flipped. For $\alpha = 0°$, the mode is excited at $f = 0.97$Hz, which is consistent with the bending mode, and for $\alpha = 90°$, the mode is excited at $f = 0.72$Hz, which corresponds to the pinwheel mode. This happens because the Y and Z axes are $90°$ apart perpendicularly to the rotation axis of the solar arrays. Therefore, the response of these two axes is equivalent to each other with an offset of $90°$.

Another important analysis relates to the gain and phase margins of the system. Table 4 summarizes each axis's minimum gain and phase margins since they depend on the solar array orientation. As expected, the minimum gain and phase margins for the Y and Z axes happen 90 degrees apart.

Table 4: Minimum gain and phase margins for each hub axis.

	Gain [dB]	SA Angle [°]	Phase [°]	SA Angle [°]
X axis	15.26	0	78.94	0
Y axis	36.48	0	81.97	90
Z axis	36.48	90	81.82	0

According to NASA's Technical Standards System,[14] the controller stability margins requirements state that "The Attitude Control System (ACS) shall have stability margins of at least 6db for rigid body stability with 30 degrees phase margin". Looking at Table 4, it is clear that these requirements are met and that the gains chosen are adequate for this spacecraft and corresponding flexible modes.

Closed-Loop Analysis

The closed-loop analysis focuses on the frequency response of the closed-loop transfer function. This is performed through Bode plots, shown in Figure 4 for each axis. As expected, the system tracks low frequencies very well, with gains close to 0dB, corresponding to unit gain, and phase shifts of 0 degrees. However, when the system is excited at the natural frequencies of the flexible modes, the system does not track the input as well, which results in a decrease in output magnitude and a phase shift. For each axis, this behavior happens for the corresponding modes: for X, it happens at the torsional mode's natural frequency, whereas for Y and Z, it happens at the bending and pinwheel natural frequencies. When the solar array angles change, the coupling between these latter modes is also present in the system's closed-loop response. Finally, the same folding and aliasing artifacts present at frequencies above 5Hz exist in the closed-loop frequency response, where the plot is not indicative of the true response of the system.

CONCLUSION

This paper provides a rigorous approach to applying frequency domain analysis to flexible spacecraft components. The equations of motion that describe the nonlinear behavior of the spacecraft are shown, which are then linearized and put into state space form. Since the input control is discrete, the continuous state space is discretized through a zero-order hold assumption, and then the Laplace transform is applied to convert from the time domain to the z domain. The frequency domain analysis approach is presented, which includes analyzing Bode plots of the open and closed-loop transfer

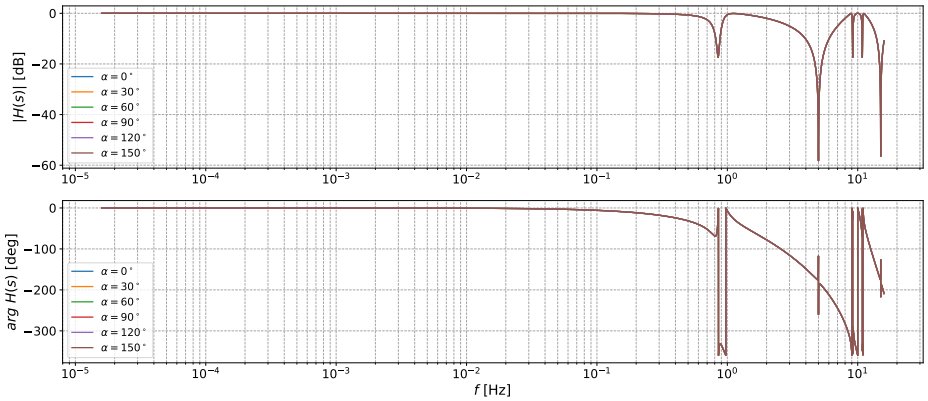

(a) Bode plot for the X axis.

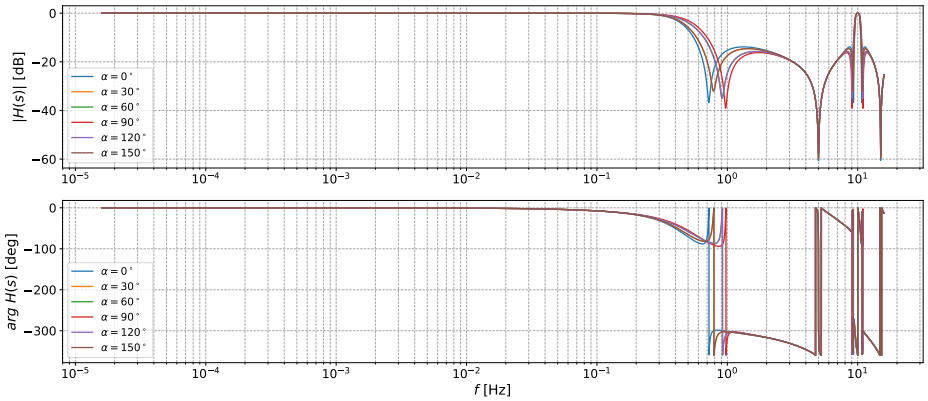

(b) Bode plot for the Y axis.

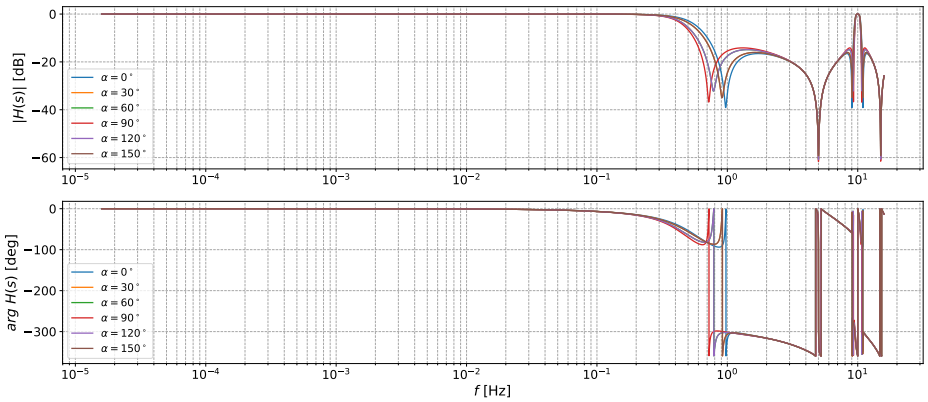

(c) Bode plot for the Z axis.

Figure 4: Bode plot of the open-loop transfer function for each axis.

functions, and extracting the gain and phase margins of the system. Finally, a comprehensive numerical example illustrates how the analysis is performed with a realistic scenario.

Future work will involve analyzing the impact of dV maneuvers on the spacecraft's behavior and comparing the flexible response with a rigid body to quantify the difference between the two.

ACKNOWLEDGMENTS

This work was supported by the La Caixa Foundation (ID 100010434) through the Postgraduate Fellowships Abroad program under agreement LCF/BQ/EU22/11930093.

REFERENCES

[1] D. C. Reynolds, *Control-Structure Interaction Mitigation for NASA's Gateway*. PhD thesis, Massachusetts Institute of Technology, 2019.

[2] Z. Bubnicki, *Modern Control Theory*. Springer, 2005.

[3] R. F. Stengel, *Optimal Control and Estimation*. Courier Corporation, 1994.

[4] H. K. Khalil, *Nonlinear Systems*. Prentice Hall, 3rd ed., 2002.

[5] H. Schaub and J. L. Junkins, *Analytical Mechanics of Space Systems*. Reston, VA: AIAA Education Series, 4th ed., 2018, 10.2514/4.105210.

[6] M. Géradin and D. J. Rixen, *Mechanical Vibrations: Theory and Application to Structural Dynamics*. John Wiley & Sons, 3rd ed., 2014.

[7] J. Vaz Carneiro, C. Allard, and H. Schaub, "Rotating Rigid Body Dynamics Architecture For Spacecraft Simulation Software Implementation," *AAS Guidance and Control Conference*, Breckenridge, CO, Feb. 2–8 2023. Paper No. AAS-23-112.

[8] J. Vaz Carneiro, C. Allard, and H. Schaub, "Effector Dynamics For Sequentially Rotating Rigid Body Spacecraft Components," *AAS/AIAA Astrodynamics Specialist Conference*, Big Sky, MT, Aug. 13–17 2023. Paper AAS 23–192.

[9] C. Allard, M. Diaz-Ramos, P. W. Kenneally, H. Schaub, and S. Piggott, "Modular Software Architecture for Fully-Coupled Spacecraft Simulations," *Journal of Aerospace Information Systems*, Vol. 15, No. 12, 2018, pp. 670–683, 10.2514/1.I010653.

[10] C. Allard, M. D. Ramos, and H. Schaub, "Computational Performance of Complex Spacecraft Simulations Using Back-Substitution," *AIAA Journal of Aerospace Information Systems*, Vol. 16, No. 10, 2019, pp. 427–436, 10.2514/1.I010713.

[11] C. Allard, S. Piggott, and H. Schaub, "Impulsive Thruster Based Attitude Stability Analysis of Spacecraft with Flexible Solar Arrays," *AAS Guidance and Control Conference*, Breckenridge, CO, Feb. 1–7 2018.

[12] D. Simon, *Optimal State Estimation: Kalman, H-infinity, and Nonlinear Approaches*. John Wiley & Sons, 2006.

[13] R. A. DeCarlo, *Linear Systems: A State Variable Approach with Numerical Implementation*. Prentice-Hall, Inc., 1989.

[14] NASA Technical Standards System, "Rules for the Design, Development, Verification, and Operation of Flight Systems," 2023.